

Microring resonator as a Rayleigh mirror for broadband laser cavity comb generation

**Aram A. Mkrtchyan¹, Anastasia S. Netrusova¹, Zohran Ali¹, Mikhail S. Mishevsky¹,
Nikita Yu. Dmitriev², Kirill N. Minkov², Dmitry A. Chermoshentsev^{2,3}, Albert G.
Nasibulin⁴, Igor A. Bilenko² and Yuriy G. Gladush^{1*}**

¹*Skolkovo Institute of Science and Technology, 30 Bolshoy Boulevard, building 1, Moscow, 121205, Russia*

²*Russian Quantum Center, 30 Bolshoy Boulevard, building 1, Skolkovo Innovation Center territory, 121205, Russia*

³*Moscow Institute of Physics and Technology, (National Research University), Dolgoprudny 141700, Russia*

⁴*Kemerovo State University, 6 Krasnaya Street, Kemerovo, 650000, Russia*

* y.gladush@skol.tech

High-quality microring resonators (MRRs) have proven to be promising sources of optical combs generated from continuous-wave radiation. In addition to the primary comb that propagates along with the pump, Rayleigh scattering creates a comb that travels in the opposite direction. Normally, the scattering is a very weak, however, in the high-quality-factor MRR the power transferred to the backward-propagating comb can be quite significant. We demonstrate that the backward-propagating comb can be used as a feedback source for a fiber laser, effectively creating a nonlinear mirror for the laser cavity. By assembling a simple laser cavity comprising only active fiber and two mirrors, one of which is an integrated MRR, we show a robust self-starting comb generation with width exceeding 500 nm. We confirm the universal character of this approach for other types of microresonators, including whispering gallery mode resonators, by launching self-starting laser cavity combs with the crystalline toroidal cavity, coupled with a tapered fiber. This method provides significant simplification for the filter-driven laser cavity soliton generation, especially when free-space coupling is applied.

Introduction

The advancements in optical frequency combs generation^{1–4} using high-quality (high-Q) microring resonators (MRRs) have given rise to numerous breakthroughs in metrology^{5–14}, spectroscopy^{15,16}, communications^{17–20}, as well as in quantum computing²¹, quantum data processing²², quantum sources^{23,24}, etc. For many applications, it is crucial to generate coherent frequency combs that, in the time domain, form dissipative cavity solitons – solitary waves that self-balance nonlinear phase shift, dispersion, losses, and energy flow^{25–30}. However, on-chip soliton generation still faces serious challenges for practical implementation. The traditional method of soliton generation involves catching the soliton “step” by scanning through the cavity resonance with a narrow-line laser. This procedure is nontrivial, prohibits self-starting^{27,31–33} and suffers from low pump-to-comb conversion efficiency, which typically does not exceed 5% for bright solitons^{30,34–36}.

To overcome these limitations, several approaches have been suggested, which can be divided into those that modify the microcavity and those that couple the pump laser to the cavity through optical feedback. Recently, Helgason *et al.* have demonstrated a technique to induce a controllable frequency shift in a selected cavity resonance by using two linearly coupled anomalous-dispersion microresonators, achieving conversion efficiency of 50%³⁷. To address the self-starting challenge, Yu *et al.* proposed an edgeless photonic crystal resonator, which enabled spontaneous soliton formation in place of Turing patterns³⁸. Another common but intricate technique is to pump the MRR with an electro-optically modulated continuous wave (CW) external laser at a precisely selected frequency. This method was successfully demonstrated with a lithium niobate platform in 2021³⁹. A popular and effective approach is the self-injection locking technique, which provides self-starting soliton comb generation^{11,40–44} with up to 40% CW to soliton comb conversion efficiency⁴⁰. Briefly, the laser diode locks to the traveling wave in the microcavity through the back-propagating wave emerging from Rayleigh scattering in the cavity⁴⁵. This approach, besides cavity-soliton generation, is commonly used for narrow linewidth, low noise, and frequency-stabilized laser generation^{46–49}.

Another elegant technique that simultaneously solves both problems of low energy conversion and self-starting is the integration of a microcavity into a fiber laser resonator, which was first demonstrated to achieve stable ultrafast mode-locking in 2012⁵⁰. By merging the fiber laser and microcavity, Bao *et al.* demonstrated 50-nm-wide laser cavity-soliton combs with 75% power in the comb⁵¹. Recently Maxwell *et al.* demonstrated that this system can exhibit self-starting soliton generation, which is naturally robust to the system perturbations and can spontaneously recover after disruption, which was

explained by interplay between slow erbium fiber gain saturation and cavity thermal shift⁵². In these works, the authors used a four-port ring resonator inside the fiber laser ring cavity. Emission from fiber laser propagated through one bus waveguide to the microcavity and returned from the drop-port to the laser cavity through the other bus waveguide.

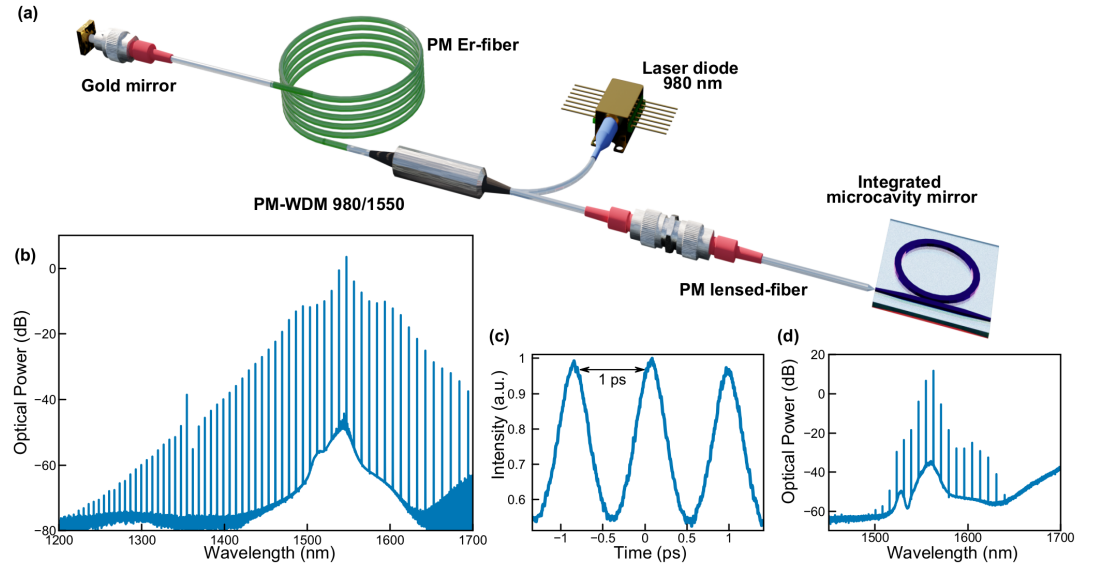
In this work, we further develop the technique of laser cavity soliton generation by demonstrating that a high-Q microring resonator can work as a nonlinear reflective mirror of the fiber laser cavity. Indeed, it has been shown that weak Rayleigh scattering into the mode of the resonator can be enhanced by an analog of the Purcell factor, leading to the formation of a back-propagating wave in the cavity and, under certain conditions, convert a major part of the pump power into it^{53,54}. The spontaneous back propagating wave formation was previously employed to enable self-injection locking where even a small reflected power is sufficient to provide an optical feedback to a laser. In the present work we demonstrate that the resonant back scattering from a MRR, working as a frequency selective mirror, can provide sufficiently large optical feedback to form a cavity for a fiber laser generation, leading to more than 500-nm-wide self-starting comb formation. This approach allows us to use a single bus waveguide MRR, which simplifies the fabrication and reduces losses compared to four-port cavity coupling, thereby maintaining the loaded Q-factor at higher level resulting in comb formation with better spectral properties. To prove the general applicability of this approach, in addition to integrated MRR, we also demonstrate the self-starting comb generation for a crystalline MgF₂ microcavity coupled with tapered fiber. This approach can be very efficient for robust laser cavity comb generation with microcavities that requires coupling from free space through prism or tapered fibers or when MRR is combined on the same photonic circuit with integrated amplifier⁵⁵⁻⁵⁸.

Results

The backward-propagating wave formation is a complex process defined by the relation between microring resonator parameters, namely, intrinsic loss (κ_0), coupling rate (κ_C), and backward-wave coupling rate (γ)⁵⁴. We have chosen the MRR with 1 THz free spectral range (FSR), nearly 1 million Q-factor, - 600 fs²/mm second-order dispersion, and following relation between its parameters: $\kappa_0 < \kappa_C < \gamma < \kappa_0 + \kappa_C$ (see the characterization section for details). This relation guaranties prominent back propagating wave in linear regime without significant mode splitting. When the power is enough for comb formation, the nonlinear interaction between the clockwise and counterclockwise waves comes into play, giving rise to rich phenomena such as modulation instability, intermode hopping, and spontaneous symmetry breaking⁵⁹⁻⁶¹. We checked that under external tunable CW laser pump a back-propagating comb is formed in MRR with a spectrum similar to forward propagating (Figure S1).

We used the MRR to form a fiber laser cavity by edge-coupling the chip with the MRR to the polarization maintaining (PM) Er-doped fiber amplifier (EDFA) and introducing fully reflecting gold mirror on the other side (see Figure 1a).

Additionally, the cavity includes a PM-WDM with a 980 nm laser diode and a pair of fiber connectors for simplifying coupling alignment. The total laser cavity length is 3.2 m, corresponding to a 32.5 MHz FSR. It is several times smaller compared to the MRR resonance width of 270 MHz. At the threshold pump power of 43 mW, laser generation starts at the wavelength of one of the resonances due to build up of the back propagating wave in the MRR. As the pump power increases, the optical comb grows, reaching its maximum width of more than 500 nm at the maximum available pump power of 500 mW, corresponding to 91 mW in the fiber before the chip (Figure 1b). Remarkably, turning the laser off and on led to the immediate recovery of the comb (see Supplementary video). This behavior is similar to laser cavity solitons, demonstrated earlier with a four-port cavity nested into fiber laser, where the soliton was manifested as a stable attractor due to the interaction of slow gain saturation and MRR heating⁵². To investigate the temporal characteristics, we had to amplify the signal with a commercial amplifier and carried out autocorrelation measurements. The amplification significantly distorted the signal, limiting amplified comb to 15 nm at the 3 dB level (see Figure 1d) and presumably widening the pulse. The autocorrelation trace clearly showed overlapping ultrashort pulses with a 1 ps period, corresponding



to 1 THz repetition rate inside MRR (see Figure 1c).

Figure 1. Generation of broadband frequency combs using high-Q silicon nitride (Si_3N_4) microresonator nested into fiber laser cavity in reflection scheme. a) Schematic illustration of the fiber laser with integrated photonic chip for cavity soliton generation: one-meter-long polarization-maintaining Er-fiber pumped with 980 nm laser diode through a broadband wavelength-division multiplexer 980/1550 nm (PM-WDM). All fibers in the system were polarization-maintained and exhibited a second order dispersion of $-23 \text{ fs}^2/\text{mm}$. Lensed fibers are used to couple light to the chip. Si_3N_4 microring resonator has 1 THz repetition rate, nearly 1 million Q-factor and anomalous dispersion. b) Cavity soliton spectrum with width exceeding 500 nm at 112 mW intracavity

power. c) Autocorrelation trace after external amplification with 1 THz repetition rate pulse sequence and d) comb spectrum after external amplifier.

We note that our scheme does not include an optical filter and a delay line, which are usually presented in such systems^{50–52,62,63}. We found that, in our case, these elements have a very small effect on the generation performance, and we eliminated them from the cavity. A brief discussion can be found in the Supplementary Materials (see section SM2).

To investigate the fiber intracavity dynamics of the comb, we introduced a 2x2 70/30 coupler into the fiber resonator (see Figure S4), which allows us to track the intracavity back-reflected and amplified combs. It introduces additional losses to the system, reducing the intracavity power, but the general behavior is preserved. The optical spectra for transmitted and reflected combs (Figures 2a and 2b) demonstrate slight differences while maintaining the triangular shape typical for soliton combs. The apparent reduction in the reflected comb width arises from additional losses at the coupler and circulator located on the way to a photodetector. Figure 2c shows the comb after propagation through the EDFA, demonstrating significant amplification within the erbium gain spectrum region. Autocorrelation traces clearly show the pulse train at all three points under consideration (insets of Figures 2a-c).

To prove soliton comb operation, we carried out measurements of the comb modes detuning using laser scanning spectroscopy (LSS) technique^{51,62}. We introduced external tunable 10 kHz linewidth CW laser emission into the fiber cavity through the fiber optic circulator attached to the additional 70/30 coupler (see section SM3 in Supplementary materials). The CW laser swept through one of the MRR “hot” resonances simultaneously with comb generation. For the well-formed comb of Fig. 2a, the beating modes (Fig. 2d-f,) clearly indicate the red shift of the central and two side modes with respect to cavity resonance, indicating that the system may operate in the soliton regime^{64,65}. It is important to note that 270 MHz linewidth of the MRR resonance should include several laser modes with 32.5 MHz FSR. Nevertheless, we observe only one laser mode inside each resonance. We conclude that laser operates on a single supermode, i.e. a sequence of equidistant laser modes with 1 THz separation, which is also evidence for pulsed generation with 1 THz repetition rate.

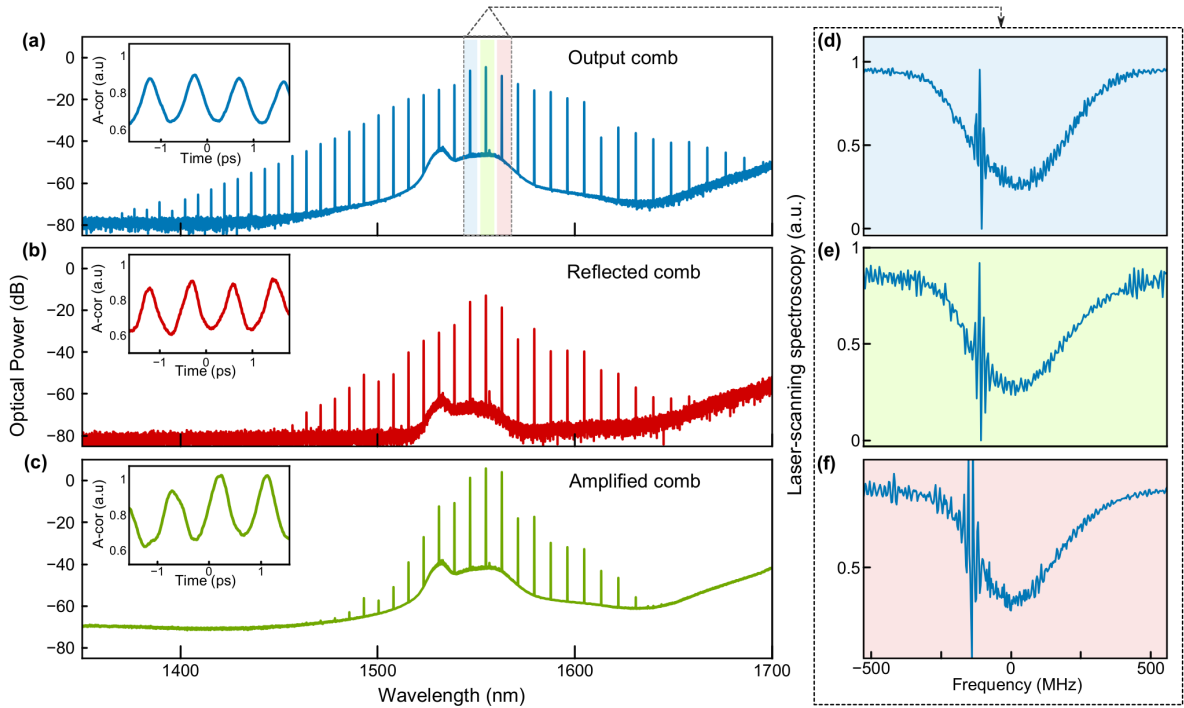


Figure 2. Single soliton comb generation in hybrid-laser scheme. a) Output, b) reflected, and c) amplified comb spectra and their corresponding autocorrelation traces in the insets, d-f) laser-scanning spectroscopy of the 1542 nm (d), 1554 nm (e), and 1562 nm (f) microcavity resonances measured for an output comb. All plots indicate red-detuned state for a central and side modes of the comb.

Next, we measure pump power-dependent spectrum, mode-detuning, and fiber intracavity power simultaneously at the chip, as well as reflected and transmitted positions as indicated on Fig. S4. The power entering the bus waveguide (green line in Fig. 3a) shows a linear dependence on the pump power. This power is converted into forward-propagating comb (blue area) and backward-propagating comb (red area), while the rest of the power (green area) corresponds mainly to losses in the MRR. Additionally, we observe that the transmitted and reflected combs exhibit a nonlinear dependence on the pump power.

To investigate the comb formation in more detail, in Figure 3b we plot the power fractions of transmitted (blue line) and reflected (red line) combs, as well as corresponding mode detunings as a function of power inside the bus waveguide. The corresponding comb spectra are shown in Fig. 3c. Below the lasing threshold, almost all the power is transmitted, while a small reflection of the order of 1% can be attributed to the reflection from the chip facet (see Fig. S4 for the fractions of transmitted and reflected light measured in the fibers). As the power inside the waveguide approaches 1 mW, a rapid growth of reflection to 48% is observed, accompanied by the drop in the transmitted signal to 10%. LSS measurements show that at CW state the laser mode is blue-detuned with respect to the MRR resonance. However, as the power increases and the

comb is excited, the laser supermode shifts to a red-detuned state. This behavior resembles the comb formation observed in the filter-driven four-wave mixing setup reported by Rowley *et al.*⁵², with the notable difference that the multiple soliton formation is never observed for this MRR at the available pump power. Interestingly, as the comb develops, a significant drop in the reflected signal to 23% is observed, along with an increase in the transmitted comb power fraction to 36%. We attribute this behavior to the nonlinear interaction between forward and backward-propagating waves through the cross-phase modulation^{59,66}. Additionally, the fraction of light lost in the MRR can be determined by summing the fractions of transmitted and reflected light (orange line in Fig. 3b). Once the pump power is sufficient to form a CW laser line, the losses approach 40% and remain near this value independently of the pump power. The gradual change in losses resembles the shift of the laser supermode through the MRR resonances with the maximum losses corresponding to the supermode position at the resonance minimum.

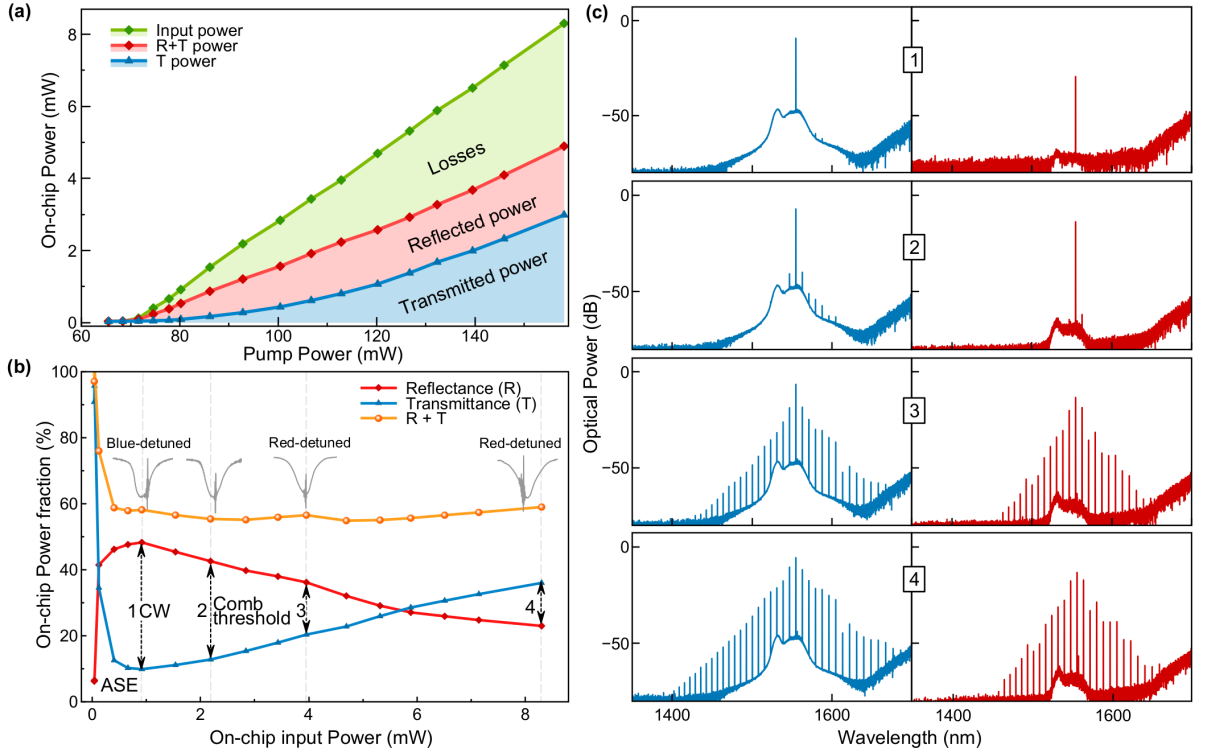


Figure 3. Intracavity dynamic measurements. (a) Power measured in the fiber for the transmitted and reflected combs, as well as the power propagated after a double EDFA pass, plotted as a function of pump power. (b) Chip reflection (red) and transmission (blue) as a function of the power in the bus waveguide. The brown line demonstrates the sum of transmitted and reflected signals, indicating nearly 40% losses in the chip. Numbers correspond to the spectra shown in (c) for different pump powers for transmitted (blue) and reflected (red) combs.

The reflection from the chip facet, reaching 1%, is sufficient to start CW laser generation even without the MRR. This raises the question whether it affects the generation starting dynamics and whether starting mechanism similar to self-injection locking could be responsible here⁴³. To prove that comb generation self-starting can be achieved solely with a high-Q MRR mirror, we replaced the chip with a crystalline toroidal microresonator (MgF₂; 10⁹ Q-factor, 35 GHz FSR and normal dispersion) coupled through a tapered fiber (see Figure 4a). The relatively thick taper with a 3 μm waist was prepared to ensure the parasitic reflection fraction is below 10⁻⁵. The response of the system to the pump power generally resembles the behavior observed with the integrated MRR. The reflected power from the toroidal resonator as a function of the power incident from the active fiber is shown in Figure 4b. When the incident power reaches 3 mW (86 mW pump power) the reflection rapidly changes to 0.1%, accompanied by the formation of CW laser emission (see insets in Fig.4b for spectra). Further increasing pump power leads to comb formation^{48,67-69}. The system also demonstrates self-starting behavior, which resembles, even if the pump power is turned off and on. However, we did not manage to achieve a coherent comb state with this approach. Instead, the comb always consists of several subcombs corresponding to different families of toroidal cavity resonances⁷⁰. A more detailed investigation of the generation regimes in a fiber laser with a nested crystalline resonator is left for future work.

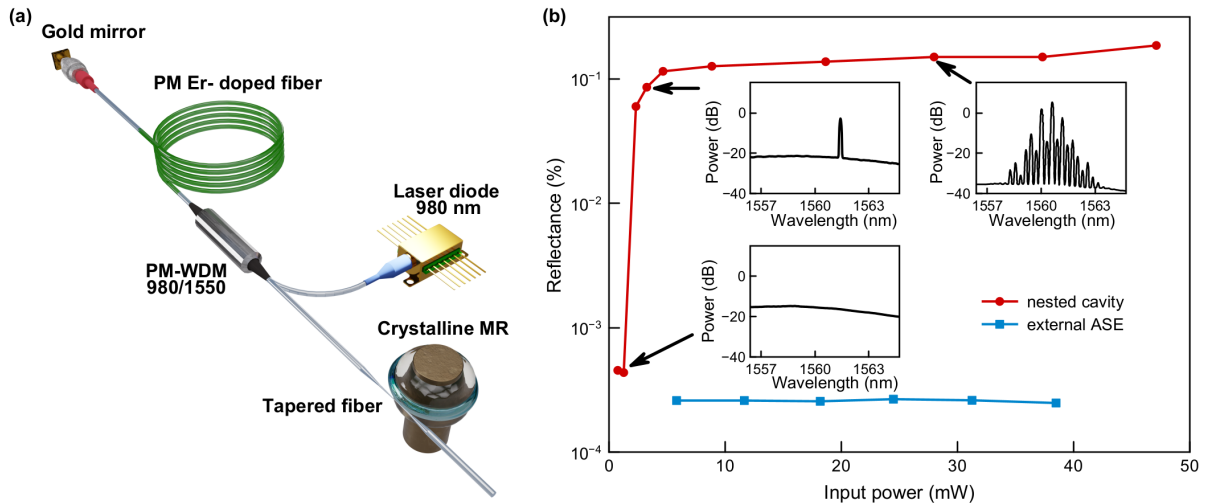


Figure 4. Generation of frequency combs using high-Q MgF₂ crystalline toroidal microresonator nested into fiber cavity, where only backward light propagation due to Rayleigh scattering create feedback. a) Hybrid-laser scheme with the crystalline MgF₂ MRR with 10⁹ Q-factor, 35 GHz FSR and normal dispersion, was used to generate whispering gallery modes. b) Reflection from crystalline microcavity as a function of power incident from the active fiber (red curve). The corresponding spectra are shown in the insets. Blue curve shows the reflection from an external amplified spontaneous emission (ASE) source, which is independent of the source power.

Discussion

In conclusion, we have demonstrated the application of a ring microcavity as a partially reflecting mirror to form a laser cavity for efficient and robust comb generation. In our setup, the MRR serves two functions. First, it is responsible for the comb formation from the EDFA amplified light. Second, the back-propagating comb, spontaneously created by Rayleigh scattering, provides optical feedback for the laser cavity. We used two types of the cavities – the silicon nitride integrated MRR with single bus waveguide and the toroidal crystalline microresonator coupled by the tapered fiber. In both cases, we observed robust self-starting comb formation, which demonstrates full recovery under perturbations. For the integrated MRR, we show coherent comb formation with 1 THz FSR and width of more than 500 nm, strongly evidenced by autocorrelation measurements and red detuning of the main comb lines. This comb shows long term stability and recovers its state under external perturbations. We suggest that this method expands the applicability of previously proposed laser cavity soliton generation method and provides significant advantage when single coupling is desirable.

Materials and methods

Integrated MRR. The photonic Si_3N_4 chip was fabricated in Ligentec, Switzerland, and contains structures consisting of 25- μm radius microring resonators and bus waveguide (Figure 7a-b). All structures were fully characterized using a method based on a pre-calibrated Mach-Zehnder interferometer⁵⁴. Characterization includes measurements of the microresonator transmission spectrum (Figure 7d), microresonator dispersion landscape (e) and distributions of Q-factor, intrinsic loss $\kappa_0/2\pi$, coupling rate $\kappa_C/2\pi$ and backward-wave coupling rate (mode splitting) $\gamma/2\pi$ for all resonances in wavelength range from 1510 nm to 1620 nm (Fig. 7f). For the central line measured parameters correspond to $\kappa_0/2\pi = 95$ MHz, $\kappa_C/2\pi = 116$ MHz and $\gamma/2\pi = 142$ MHz. According to the characterization results, the microring resonator exhibits anomalous group velocity dispersion and the pump mode corresponding to the central line of the generated microcomb features $Q \sim 0.9 \times 10^6$ (Figure 7c).

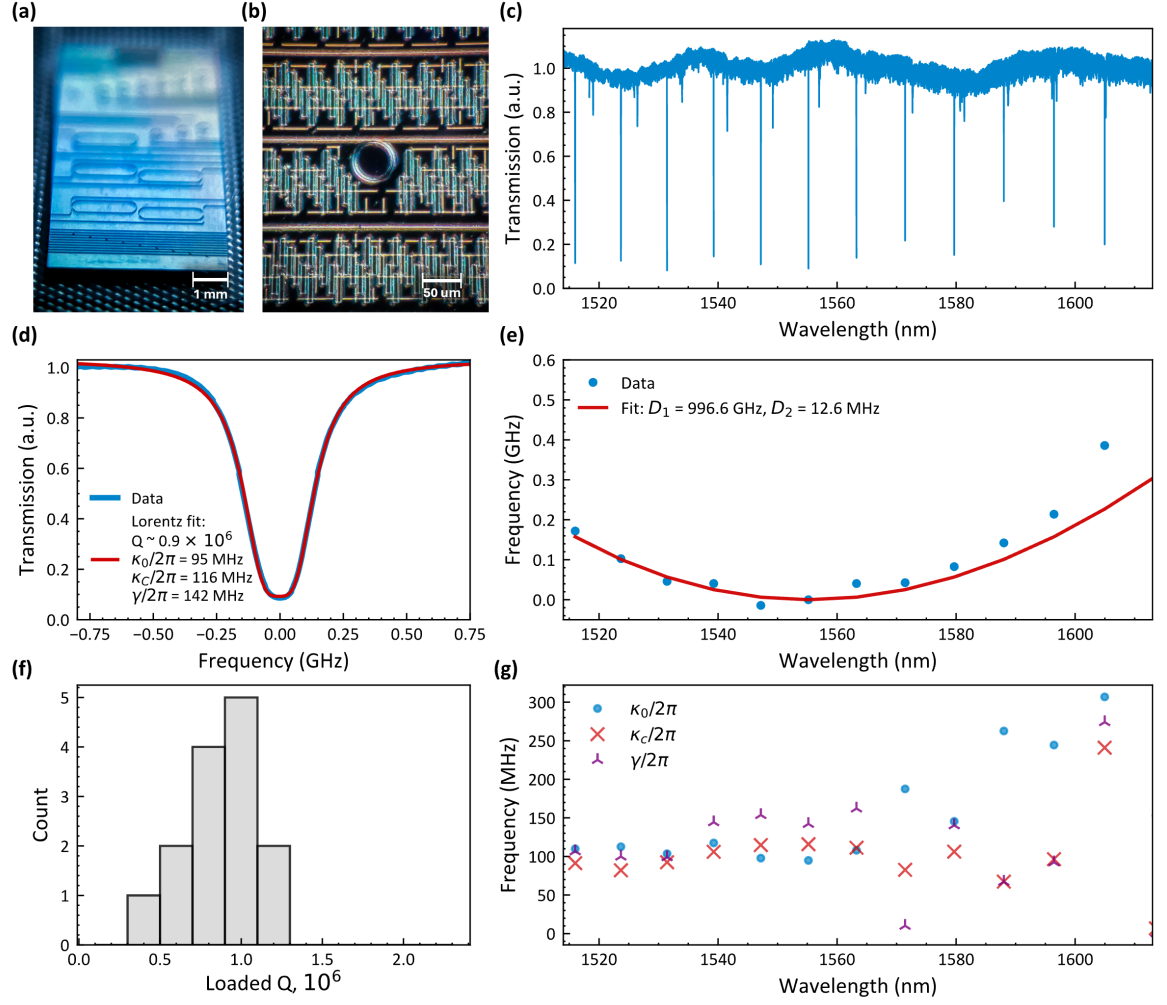


Figure 5. Characterization of the Si_3N_4 microring resonator. a) Photonic chip containing 1THz microring resonators. b) Structure under study consisting of the microring resonator and bus waveguide. c) Microresonator mode spectrum. d) Parameters of mode corresponding to the central comb line. e) Dispersion landscape (microresonator eigenfrequencies deviation from the uniform FSR-grid) f-g) Distribution histograms of the Q-factor, intrinsic loss ($\kappa_0/2\pi$), coupling rate ($\kappa_c/2\pi$), and backward-wave coupling rate (mode splitting, $\gamma/2\pi$) for microresonator modes in the range 1510–1620 nm, estimated using a Lorentzian function, with backscattering taken into account.

Measurement Technique. Laser scanning spectroscopy and chip resonant/ out-of-resonance measurements were carried out by clean sweeping narrow-linewidth tunable Pure Photonics PPCL550 laser through the circulator and the 2.5 μm waist size lensed fiber (AMS Technologies, PM-lensed fiber TPMJ-3A-1550-8/125-0.25-7-2.5-14-2-AR). For laser scanning spectroscopy, we used a Thorlabs DET08CFC/M 5 GHz photodetector and a Tektronix MDO3102 oscilloscope. Average laser power characteristics were measured by Thorlabs S132C power sensors. The spectral properties of optical frequency

comb were measured by DEVISER AE8600 and Yokogawa AQ6370E spectrum analyzers with 600 – 1700 nm operating window. The temporal characteristics of solitons was investigated with a Femtochrome FR-103XL autocorrelator with 1 fs resolution.

Fiber Laser. The fiber laser cavity shown in Fig. 2a) was assembled from the EDFA spliced to the gold mirror from on one side and edge-coupled to the MRR on the other side through the lensed fiber. All the fibers used in this work were polarization-maintaining (PM). To make the fully reflecting mirror, we sputtered gold onto the fiber ferrule, resulting in a 98% reflection coefficient. The EDFA consisted of 1-meter Liekke Er-doped active fiber with an 80 dB/m absorption coefficient at 1530 nm, pumped by 980 nm laser diode with a maximum power of 500 mW through a 1550/980 wavelength division multiplexer (1550/980 WDM). The total laser cavity length was 3.2 m, corresponding to 32.5 MHz FSR.

Crystalline microresonator. Microresonator and tapered fiber for coupling were fabricated at the Russian Quantum Center. The resonator was manufactured from magnesium fluoride using diamond turning⁷¹. The diameter of the resonator is 1.94 mm, its thickness is 1.0 mm, and the radius of curvature is 0.35 mm. The taper was produced from a single-mode fiber (SMF28 Ultra) using a hydrogen flame⁷².

Acknowledgments. The research was supported by *RSF* (project No. 25-22-00388).

Data availability. The data that support the plots within this paper and other findings of this study are available from the corresponding author upon reasonable request.

Corresponding author. Correspondence to Yuriy Gladush.

Author contributions. Y.G.G., I.A.B., A.A.M. developed the original research idea and designed the experiment. A.A.M., Z.A., A.S.N., N.Y.D. performed the experiment and analyzed the data for integrated chip, K.N.M., M.S.M. performed the experiment and analyzed the data for crystalline resonator. All authors contributed to results discussion and experiment setting. A.A.M., A.S.N. drafted the manuscript, Y.G.G., I.A.B., D.A.C. contributed to manuscript writing. Y.G.G., A.G.N., I.A.B. supervised the research.

Competing interests. The authors declare no competing interests.

References

1. Kippenberg, T. J., Holzwarth, R. & Diddams, S. A. Microresonator-based optical frequency combs. *Science (1979)* **332**, 555–559 (2011).
2. Kippenberg, T. J., Gaeta, A. L., Lipson, M. & Gorodetsky, M. L. Dissipative Kerr solitons in optical microresonators. *Science (1979)* **361**, (2018).
3. Pasquazi, A. *et al.* Micro-combs: A novel generation of optical sources. *Phys Rep* **729**, 1–81 (2018).
4. Fortier, T. & Baumann, E. 20 Years of Developments in Optical Frequency Comb Technology and Applications. *Commun Phys* **2**, 153 (2019).
5. Savchenkov, A. A. *et al.* Stabilization of a Kerr frequency comb oscillator. *Opt Lett* **38**, 2636 (2013).
6. Papp, S. B. *et al.* Microresonator frequency comb optical clock. *Optica* **1**, 10 (2014).
7. Del’Haye, P. *et al.* Phase-coherent microwave-to-optical link with a self-referenced microcomb. *Nat Photonics* **10**, 516–520 (2016).
8. Brasch, V., Lucas, E., Jost, J. D., Geiselmann, M. & Kippenberg, T. J. Self-referenced photonic chip soliton Kerr frequency comb. *Light Sci Appl* **6**, (2017).
9. Stern, L. *et al.* Direct Kerr frequency comb atomic spectroscopy and stabilization. *Sci Adv* **6**, (2020).
10. Li, B. *et al.* Reaching fiber-laser coherence in integrated photonics. *Opt Lett* **46**, 5201 (2021).
11. Liang, W. *et al.* High spectral purity Kerr frequency comb radio frequency photonic oscillator. *Nat Commun* **6**, (2015).
12. Lei, F. *et al.* Optical linewidth of soliton microcombs. *Nat Commun* **13**, (2022).
13. Jin, W. *et al.* Hertz-linewidth semiconductor lasers using CMOS-ready ultra-high-Q microresonators. *Nat Photonics* **15**, 346–353 (2021).
14. Volyanskiy, K. *et al.* Compact optoelectronic microwave oscillators using ultra-high Q whispering gallery mode disk-resonators and phase modulation. *Opt Express* **18**, 22358 (2010).
15. Yu, M. *et al.* Silicon-chip-based mid-infrared dual-comb spectroscopy. *Nat Commun* **9**, 1869 (2018).
16. Suh, M. G., Yang, Q. F., Yang, K. Y., Yi, X. & Vahala, K. J. Microresonator soliton dual-comb spectroscopy. *Science (1979)* **354**, (2016).
17. Marin-Palomo, P. *et al.* Microresonator-based solitons for massively parallel coherent optical communications. *Nature* **546**, 274–279 (2017).

18. Pfeifle, J. *et al.* Optimally coherent Kerr combs generated with crystalline whispering gallery mode resonators for ultrahigh capacity fiber communications. *Phys Rev Lett* **114**, (2015).
19. Hu, H. *et al.* Single-source chip-based frequency comb enabling extreme parallel data transmission. *Nat Photonics* **12**, 469–473 (2018).
20. Corcoran, B. *et al.* Ultra-dense optical data transmission over standard fibre with a single chip source. *Nat Commun* **11**, (2020).
21. Menicucci, N. C., Flammia, S. T. & Pfister, O. One-way quantum computing in the optical frequency comb. *Phys Rev Lett* **101**, 130501 (2008).
22. Lu, H. H., Weiner, A. M., Lougovski, P. & Lukens, J. M. Quantum Information Processing with Frequency-Comb Qudits. *IEEE Photonics Technology Letters* **31**, 1858–1861 (2019).
23. Kues, M. *et al.* On-chip generation of high-dimensional entangled quantum states and their coherent control. *Nature* **546**, 622–626 (2017).
24. Reimer, C. *et al.* Generation of multiphoton entangled quantum states by means of integrated frequency combs. *Science (1979)* **351**, 1176–1180 (2016).
25. Herr, T. *et al.* Temporal solitons in optical microresonators. *Nature Photonics* **2013** 8:2 **8**, 145–152 (2013).
26. Haelterman, M., Trillo, S. & Wabnitz, S. Dissipative modulation instability in a nonlinear dispersive ring cavity. *Opt Commun* **91**, 401–407 (1992).
27. Leo, F. *et al.* Temporal cavity solitons in one-dimensional Kerr media as bits in an all-optical buffer. *Nat Photonics* **4**, 471–476 (2010).
28. Xue, X. *et al.* Mode-locked dark pulse Kerr combs in normal-dispersion microresonators. *Nat Photonics* **9**, 594–600 (2015).
29. Cole, D. C., Lamb, E. S., Del’Haye, P., Diddams, S. A. & Papp, S. B. Soliton crystals in Kerr resonators. *Nat Photonics* **11**, 671–676 (2017).
30. Xue, X., Wang, P. H., Xuan, Y., Qi, M. & Weiner, A. M. Microresonator Kerr frequency combs with high conversion efficiency. *Laser Photon Rev* **11**, 1600276 (2017).
31. Barland, S. *et al.* Temporal localized structures in optical resonators. *Adv Phys X* **2**, 496–517 (2017).
32. Firth, W. Temporal cavity solitons: Buffering optical data. *Nat Photonics* **4**, 415–417 (2010).
33. Marconi, M., Javaloyes, J., Balle, S. & Giudici, M. How lasing localized structures evolve out of passive mode locking. *Phys Rev Lett* **112**, (2014).

34. Wang, P. H. *et al.* Intracavity Characterization of Micro-comb Generation in the Single Soliton Regime. *Optics InfoBase Conference Papers* **24**, 10890 (2016).
35. Bao, C. *et al.* Nonlinear conversion efficiency in Kerr frequency comb generation. *Opt Lett* **39**, 6126 (2014).
36. Li, M. *et al.* Breaking the efficiency limitations of dissipative Kerr solitons using nonlinear couplers. *Sci China Phys Mech Astron* **67**, 1–7 (2024).
37. Helgason, Ó. B. *et al.* Surpassing the nonlinear conversion efficiency of soliton microcombs. *Nature Photonics* **2023 17:11** **17**, 992–999 (2023).
38. Yu, S. P. *et al.* Spontaneous pulse formation in edgeless photonic crystal resonators. *Nature Photonics* **2021 15:6** **15**, 461–467 (2021).
39. He, Y. *et al.* Self-starting bi-chromatic LiNbO₃ soliton microcomb. *Optica* **6**, 1138 (2019).
40. Dmitriev, N. Y. *et al.* Hybrid Integrated Dual-Microcomb Source. *Phys Rev Appl* **18**, (2022).
41. Stern, B., Ji, X., Okawachi, Y., Gaeta, A. L. & Lipson, M. Battery-operated integrated frequency comb generator. *Nature* **562**, 401–405 (2018).
42. Shen, B. *et al.* Integrated turnkey soliton microcombs. *Nature* **582**, 365–369 (2020).
43. Voloshin, A. S. *et al.* Dynamics of soliton self-injection locking in optical microresonators. *Nat Commun* **12**, 1–10 (2021).
44. Lihachev, G. *et al.* Platicon microcomb generation using laser self-injection locking. *Nat Commun* **13**, 1771 (2022).
45. Gorodetsky, M. L., Pryamikov, A. D. & Ilchenko, V. S. Rayleigh scattering in high-Q microspheres. *Journal of the Optical Society of America B* **17**, 1051 (2000).
46. Dahmani, B., Hollberg, L. & Drullinger, R. Frequency stabilization of semiconductor lasers by resonant optical feedback. *Opt Lett* **12**, 876 (1987).
47. Su, Q. *et al.* A Self-Injection Locked Laser Based on High-Q Micro-Ring Resonator with Adjustable Feedback. *Journal of Lightwave Technology* **41**, 6756–6763 (2023).
48. Galiev, R. R., Kondratiev, N. M., Lobanov, V. E., Matsko, A. B. & Bilenko, I. A. Optimization of Laser Stabilization via Self-Injection Locking to a Whispering-Gallery-Mode Microresonator. *Phys Rev Appl* **14**, 014036 (2020).
49. Liang, W. *et al.* Ultralow noise miniature external cavity semiconductor laser. *Nat Commun* **6**, (2015).

50. Peccianti, M. *et al.* Demonstration of a stable ultrafast laser based on a nonlinear microcavity. *Nature Communications* 2012 3:1 **3**, 1–6 (2012).
51. Bao, H. *et al.* Laser cavity-soliton microcombs. *Nat Photonics* **13**, 384–389 (2019).
52. Rowley, M. *et al.* Self-emergence of robust solitons in a microcavity. *Nature* **608**, 303–309 (2022).
53. Mazzei, A. *et al.* Controlled coupling of counterpropagating Whispering-Gallery modes by a single rayleigh scatterer: A classical problem in a quantum optical light. *Phys Rev Lett* **99**, 173603 (2007).
54. Kippenberg, T. J., Vahala, K. J. & Spillane, S. M. Modal coupling in traveling-wave resonators. *Optics Letters*, Vol. 27, Issue 19, pp. 1669-1671 **27**, 1669–1671 (2002).
55. Liu, Y. *et al.* A photonic integrated circuit-based erbium-doped amplifier. *Science* (1979) **376**, 1309–1313 (2022).
56. Rönn, J. *et al.* Ultra-high on-chip optical gain in erbium-based hybrid slot waveguides. *Nat Commun* **10**, 432 (2019).
57. Frankis, H. C. *et al.* Erbium-doped TeO₂-coated Si₃N₄ waveguide amplifiers with 5 dB net gain. *Photonics Res* **8**, 127 (2020).
58. Van Gasse, K., Wang, R. & Roelkens, G. 27 dB gain III–V-on-silicon semiconductor optical amplifier with > 17 dBm output power. *Opt Express* **27**, 293 (2019).
59. Wang, X. *et al.* Experimental Demonstration of Self-Oscillation Microcomb in a Mode-Splitting Microresonator. *Front Phys* **10**, 908141 (2022).
60. Kondratiev, N. M. & Lobanov, V. E. Modulational instability and frequency combs in whispering-gallery-mode microresonators with backscattering. *Phys Rev A (Coll Park)* **101**, 013816 (2020).
61. Matsko, A. B. & Maleki, L. Bose-Hubbard hopping due to resonant Rayleigh scattering. *Optics Letters*, Vol. 42, Issue 22, pp. 4764-4767 **42**, 4764–4767 (2017).
62. Bao, H. *et al.* Turing patterns in a fiber laser with a nested microresonator: Robust and controllable microcomb generation. *Phys Rev Res* **2**, (2020).
63. Cutrona, A. *et al.* Nonlocal bonding of a soliton and a blue-detuned state in a microcomb laser. *Commun Phys* **6**, 1–10 (2023).
64. Yi, X. *et al.* Soliton frequency comb at microwave rates in a high-Q silica microresonator. *Optica* **2**, 1078 (2015).
65. Herr, T. *et al.* Temporal solitons in optical microresonators. *Nat Photonics* **8**, 145–152 (2014).

66. Xu, G. *et al.* Spontaneous symmetry breaking of dissipative optical solitons in a two-component Kerr resonator. *Nature Communications* 2021 12:1 **12**, 1–9 (2021).
67. Pavlov, N. G. *et al.* Soliton dual frequency combs in crystalline microresonators. *Opt Lett* **42**, 514 (2017).
68. Shitikov, A. E. *et al.* Microresonator and Laser Parameter Definition via Self-Injection Locking. *Phys Rev Appl* **14**, 064047 (2020).
69. Shitikov, A. E. *et al.* Optimization of laser stabilization via self-injection locking to a whispering-gallery-mode microresonator: experimental study. *Opt Express* **31**, 313 (2023).
70. Yu, N. & Grudin, I. S. Dispersion engineering of crystalline resonators via microstructuring. *Optica*, Vol. 2, Issue 3, pp. 221-224 **2**, 221–224 (2015).
71. Min'kov, K. N. *et al.* Fabrication of high-Q crystalline whispering gallery mode microcavities using single-point diamond turning. *Journal of Optical Technology*, Vol. 88, Issue 6, pp. 348-353 **88**, 348–353 (2021).
72. Min'kov, K. N. *et al.* An Automated Setup for the Manufacture of Tapered Optical Fibers with a Submicron Diameter. *Instruments and Experimental Techniques* **67**, 390–397 (2024).